phys. stat. sol. (a) **122**, 413 (1990)

Subject classification: 73.40; 85; S8.15

Department of Physics, Humboldt University, Berlin[1])

Spatially Variable Drift Mobility Model for $Hg_{1-x}Cd_xTe$ Diodes

I. Analytical Base and Fit to Hall Data

By

A. SCHENK

A microscopic model of the drift mobility in $Hg_{1-x}Cd_xTe$ ($x \approx 0.2$) is established on the basis of the Kohler variational method. The relevant scattering mechanisms, degeneracy, Kane band structure, and structural point defects are included. The dependence of the electron mobility on the Fermi level position is investigated. The model is compared with experimental Hall data taking into account calculated Hall factors. The spatial variability of electron and heavy hole drift mobilities in a $1Dn^+n^-p$-junction diode is demonstrated. The mobility routine, which can easily be modified for other materials, will be applied in a 2D device simulation package.

Ein mikroskopisches Modell der Driftbeweglichkeit in $Hg_{1-x}Cd_xTe$ ($x \approx 0{,}2$) wird auf der Grundlage des Kohlerschen Variationsverfahrens abgeleitet. Die relevanten Streumechanismen, Entartung, Kane-Bänder und strukturelle Punktdefekte werden berücksichtigt. Die Abhängigkeit der Elektronen-Beweglichkeit von der Lage des Fermi-Niveaus wird untersucht. Das Modell wird mit Messungen der Hall-Beweglichkeit unter Einschluß berechneter Hall-Faktoren verglichen. Die Ortsabhängigkeit der Driftbeweglichkeit von Elektronen und schweren Löchern wird anhand einer n^+n^-p-Diode demonstriert. Das Beweglichkeitsprogramm, das leicht für andere Materialien modifiziert werden kann, ist für den Einsatz in der numerischen 2D Bauelemente-Simulation vorgesehen.

1. Introduction

In $Hg_{1-x}Cd_xTe$ the drift mobility is a function of the local carrier density not only due to the screening of the Coulomb interaction but also due to degeneracy effects. In the latter case all scattering processes depend directly on the position of the Fermi level. Consequently, the simple factorization of the conductivity into carrier density and constant mobility, as is used commonly in device simulation, fails.

In this paper a microscopic mobility model $\mu(T, x, N_{dop}(\bar{r}), n(r), p(r))$ will be described that takes into account all relevant scattering mechanisms in $Hg_{1-x}Cd_xTe$ with $x \approx 0.2$ on the basis of the Kohler variational method. That enables to handle the optical-phonon scattering, to consider degeneracy and Kane band structure, and to restrict the numerical expense to a level suitable for application in device simulation packages. By changing certain parameters this model can be used also for other materials.

Section 2 will state the analytical basis and some limitations of the model. In Section 3 the most important material functions and parameters used will be given. The theoretical

[1]) Invalidenstr. 110, O-1040 Berlin, FRG.

results are fitted then to experimental Hall data in Section 4, paying attention to the Hall factor. In Section 5 the expected electron and heavy hole mobility profiles of a 1D n^+n^-p structure will be discussed.

2. Analytical Base

Scattering mechanisms considered include polar optical (po), piezoelectric (pz), and acoustic (ac) phonon modes, ionized impurity scattering (cc), neutral impurity scattering (nc), alloy scattering (dis), and strain field scattering (sf). The pz-and ac-scattering yield only small corrections to the mobility, whereas the nonpolar optical phonon modes can be neglected at all. The important but inelastic po-scattering can be treated by the Kohler variational method (for details see e.g. [1]).

The first-order result for the electron conductivity is

$$\sigma_n = -\frac{e^2 n^2}{2\hbar^2 d_0} \tag{1}$$

with the electron density n (e elementary charge). All expressions will be given for electrons only, those for light and heavy holes follow immediately from $m_c \to m_{lh,hh}$, $n \to p_{lh,hh}$, and $\xi = kT/E_g \to 0$ in the case of heavy holes. Defining the electron mobility μ_n by

$$\sigma_n = e\mu_n n\,, \tag{2}$$

a constant μ_n can only occur if $d_0 \sim n$ holds, which is approximately fulfilled in the case of Boltzmann statistics. Combining (1) and (2) one gets

$$\mu_n(n) = -\frac{en}{2\hbar^2 d_0}\,. \tag{3}$$

In (1) and (3) the quantity d_0 is defined by

$$d_0 = -\frac{1}{2\Omega kT}\sum_{\boldsymbol{k}\boldsymbol{k}'}[1 - f(E_{\boldsymbol{k}})]\, f(E_{\boldsymbol{k}'})\, W_{\boldsymbol{k}\boldsymbol{k}'}(k_x' - k_x)^2\,. \tag{4}$$

In (4) f is the Fermi function, Ω the crystal volume, and $W_{\boldsymbol{k}\boldsymbol{k}'}$ the transition probability for a transition $\boldsymbol{k} \to \boldsymbol{k}'$ in first order of perturbation theory. $W_{\boldsymbol{k}\boldsymbol{k}'}$ is given by the sum of the transition probabilities of all independent scattering processes. They have the following form:

2.1 Ionized impurity scattering

$$W^{cc}_{\boldsymbol{k}'\boldsymbol{k}} = \frac{A^{cc}}{(q^2 + \lambda^2)^2}\,\delta(E_{\boldsymbol{k}} - E_{\boldsymbol{k}'})\,, \qquad A^{cc} = \frac{2\pi N_{dop}(r)}{\hbar\Omega}\left(\frac{e^2}{\varepsilon_0\varepsilon_s}\right)^2 \tag{5}$$

with $\boldsymbol{q} = \boldsymbol{k}' - \boldsymbol{k}$, the screening length λ^{-1}, the concentration of ionized dopants N_{dop}, and the static dielectric function ε_s [1]. The screening is described in Thomas-Fermi approximation including degeneracy,

$$\lambda^2 = \frac{e^2}{\varepsilon_0\varepsilon_s}\left[\frac{d}{d\eta_c}\,n + \frac{d}{d\eta_v}\,p\right]. \tag{5'}$$

In (5') η_c and η_v are the electrochemical energies,

$$\eta_c = F_n - (E_c - e\varphi), \qquad \eta_v = E_v - e\varphi - F_p, \tag{5''}$$

with the quasi Fermi levels $F_{n,p}$, the band edge energies $E_{c,v}$, and the electrostatic potential $\varphi(r)$.

2.2 Polar-optical-phonon scattering

Taking into account HgTe- and CdTe-like longitudinal and transverse optical phonon modes [2, 3], the transition probability becomes

$$W^{po}_{k'k} = \frac{q^2}{(q^2+\lambda^2)^2}\frac{1}{2}\sum_{i=1,2}\frac{A^{po}_i}{\omega_{LOi}} \times [f_B(\omega_{LOi})\,\delta_{k',k+q}\,\delta(E_k - E_{k'} - \hbar\omega_{LOi}) + (f_B(\omega_{LOi})+1)\,\delta_{k',k-q}\,\delta(E_k - E_{k'} + \hbar\omega_{LOi})],$$

$$A^{po}_i = \frac{4(2\pi)^3 e^2 e_i^{*2}}{\Omega\Omega_0\varepsilon^2_{opt}\bar{M}} \quad [1]. \tag{6}$$

In (6) the effective charge e_i^* is determined by the lattice dielectric constant ε_{Li} according to

$$e_i^{*2} = \frac{\bar{M}\Omega_0}{4\pi}\omega^2_{TOi}\varepsilon_{Li}, \qquad \varepsilon_{Li} = (\varepsilon_s - \varepsilon_{opt})_i \quad [1], \tag{6'}$$

$\bar{M}$ denotes the averaged mass, Ω_0 the volume of the elementary cell, f_B denotes the Bose function, and ε_{opt} the optical dielectric constant.

2.3 Neutral impurity scattering

The Lucovski model [4] is used to describe scattering at the localized potential of deep neutral centers,

$$W^{nc}_{k'k} = A^{nc}\,\delta(E_k - E_{k'}), \qquad A^{nc} = \frac{2\pi N_t}{\hbar\Omega}V_0^2, \tag{7}$$

$$V_0 = 4\pi E_t r_0^3.$$

Three parameters have to be defined: E_t binding energy, N_t defect concentration, r_0 localization radius.

2.4 Strain field scattering

Static strain fields induced by neutral point defects give rise to a piezoelectric interaction. In HgCdTe this interaction can be far more efficient than the acoustic piezoelectric scattering. After [5] the transition probability is given by

$$W^{sf}_{k'k} = A^{sf}\frac{q^2}{(q^2+\lambda^2)^2}\,\delta(E_k - E_{k'}), \qquad A^{sf} = \frac{2\pi}{\hbar}\frac{N_t}{\Omega}\frac{3\times 2^{10}\pi^4}{35}\left(\frac{e\gamma_{pz}b^3}{\varepsilon_s}\right)^2, \tag{8}$$

where γ_{pz} is the piezoelectric tensor component c_{14} [6]. The parameter b^3 follows from a model of the dipole field induced by a neutral point defect [5],

$$\boldsymbol{u}(\boldsymbol{r}) = \frac{b^3 \boldsymbol{r}}{r^3}.$$

b can be written in units of the localization radius r_0: $b = \varkappa r_0$. Consequently, nc and sf scattering are correlated by two joint parameters (N_t, r_0). For $\varkappa$ values between 0.1 and 1 are expected.

2.5 Acoustic phonon scattering

Approximately [1],

$$W^{ac}_{k'k} = A^{ac}\,\delta(E_k - E_{k'}), \qquad A^{ac} = \frac{\pi E_1^2 2kT}{\Omega \varrho \hbar c_l^2}. \tag{9}$$

Here E_1 is the deformation potential constant, ϱ the density of the material, and c_l the longitudinal sound velocity.

2.6 Piezoelectric scattering

Approximately [1],

$$W^{pz}_{k'k} = A^{pz} \frac{q^2}{(q^2 + \lambda^2)^2}\,\delta(E_k - E_{k'}),$$
$$A^{pz} = \frac{64\pi^3 \gamma^2 e^2}{\varepsilon^2 \varrho \Omega \hbar} \frac{2kT}{c_l^2}, \tag{10}$$

where all quantities have been defined above.

2.7 Alloy scattering

Disorder scattering has been treated in various papers [7 to 11]. Following [11] one gets

$$W^{dis}_{k'k} = A^{dis}\,\delta(E_k - E_{k'}), \qquad A^{dis} = \frac{2\pi}{\Omega\hbar} x(1-x)\,V^2 N_0. \tag{11}$$

In (11) N_0 is the number of Hg and Cd atoms per unit volume and V the scattering matrix element (eV cm^3). Instead of V the difference between the electron affinities of the constituent crystals ΔE_c can be used: $V = \Delta E_c \Omega_0$. In (4) to (11) a Kane model is applied for the band structure E_k,

$$E_k = \begin{cases} E_c + \dfrac{E_g}{2}\left[\sqrt{1 + \dfrac{2\hbar^2 k^2}{E_g m_c}} - 1\right] & \text{for electrons,} \\ E_v - \dfrac{\hbar^2 k^2}{2m_{hh}} & \text{for heavy holes.} \end{cases} \tag{12}$$

In the scattering matrix elements the Bloch functions have been replaced by plane waves. Since $\Delta \gg E_g$ for $x \approx 0.2$ can be assumed (two-band model), one can estimate

the error in the matrix element, e.g. for an s-like wave function to be $a^2(k) \approx [1 + (1 + 2\hbar^2k^2/E_gm_c)^{-1/2}]/2$. If the Fermi level lies one energy gap above the band edge (high degeneracy) this error due to nonparabolicities in the matrix element is approximately 2/3.

Inserting the transition probabilities of the discussed scattering processes into (4) for the quantity d_0, five of six integrals can be calculated analytically. The remaining energy integral has to be solved numerically in order to account correctly for the intermediate region between the Boltzmann case and the case of total degeneracy. The result is

$$
\begin{aligned}
d_0 = \frac{\Omega m_c^2}{6(2\pi)^4\hbar^4}\int_0^\infty \mathrm{d}E\left(\frac{\mathrm{d}\gamma}{\mathrm{d}E}\right)^2\frac{\partial f}{\partial E}\Bigg\{&[A^{nc} + A^{dis} + A^{ac}]\frac{1}{2}\lambda^4\gamma^{*2}(E)\\
&+ [A^{pz} + A^{sf}]\lambda^2\left[\gamma^*(E) + \frac{\gamma^*(E)}{1+\gamma^*(E)} - 2\ln(1+\gamma^*(E))\right]\\
&+ A^{cc}\left[\ln(1+\gamma^*(E)) - \frac{\gamma^*(E)}{1+\gamma^*(E)}\right]\\
&+ \sum_{i=1,2}\frac{A_i^{po}}{\omega_{LOi}} f_B(\omega_{LOi})\frac{1-f(E+\hbar\omega_{LOi})}{1+f(E)}\frac{\left[1+2\dfrac{E+\hbar\omega_{LOi}}{E_g}\right]}{\left[1+2\dfrac{E}{E_g}\right]}\\
&\times[\lambda^2\gamma^{*1/2}(E)\gamma^{*1/2}(E+\hbar\omega_{LOi}) + g_+^i(E,\lambda)]\Bigg\}.
\end{aligned}
\tag{13}
$$

In (13) the following abbreviations were used:

$$
\gamma(E) = E\left(\frac{E}{E_g}+1\right),
$$

$$
\gamma^*(E) = \frac{4}{E_\lambda}\gamma(E), \qquad E_\lambda = \frac{\hbar^2\lambda^2}{2m_c},
$$

$$
g_+^i(E,\lambda) = 2\lambda^2\ln\left[\frac{q_{min}^2(E)+\lambda^2}{q_{max}^2(E)+\lambda^2}\right] + \lambda^4\frac{q_{max}^2(E) - q_{min}^2(E)}{(q_{max}^2+\lambda^2)(q_{min}^2+\lambda^2)},
$$

$$
q_{\substack{min\\max}}^2(E) = \frac{2m_c}{\hbar^2}[\gamma^{1/2}(E+\hbar\omega_{LOi}) \mp \gamma^{1/2}(E)]^2.
$$

A scaling mobility is introduced by

$$
\mu_{n0} = \frac{3e\hbar}{m_c kT}, \tag{14}
$$

which yields already the correct order of magnitude (e.g. for $T = 77$ K, $x = 0.2$ a value of 10^5 cm/Vs is obtained).

Finally a correction factor is determined in the following way: The conductivity resulting from the Kohler variational method is always smaller than the exact one. The exact mobility can be calculated in the high temperature limit, when the po-scattering dominates and becomes elastic. Then the relaxation time gives the correct result. Under the same conditions the Kohler variational method in first order yields a value which is smaller by a factor $9\pi/32$ [1].

Taking this into account, the final expression for the electron mobility can be written as

$$\mu_n = \frac{32}{9\pi}\,\mu_{n0}\,\frac{1}{-\dfrac{6\hbar^3}{nm_c kT}\,d_0} \tag{15}$$

with d_0 from (13).

Some limitations of the described model should be mentioned.

(i) The model does not account for conduction in an impurity band, which might be present in the case of large defect concentration. A donor band due to intrinsic structural defects resonant with the conduction band in connection with Fermi level pinning is sometimes assumed to explain the observed low electron mobilities.

(ii) A composition value $x \approx 0.2$ is connected with a gap of about 90 meV. The model fails in the case of very small or zero gap material, where the scattering theory has to be modified and other scattering processes have to be included [12, 2]. A detailed calculation was given by Szymanska and Dietl [12].

(iii) The Born approximation breaks down at low temperatures ($T \leqq 30$ K). A better theory results in high iteration expense [13] and does not suit for simulation purposes.

3. Material Functions and Parameters

Various empirical formulas for certain material functions exist in the literature. All referenced expressions in this chapter enter the mobility routine.

The energy gap (in eV) as a function of x and T is taken from Chu et al. [14],

$$E_g(x, T) = \{-0.295 + 1.87x - 0.28x^2 + 0.35x^4 + (6 - 14x + 3x^2) \times 10^{-4}\, T\}\,. \tag{16}$$

The momentum matrix element $P(x)$ (in eV cm) was given in [15] in the form

$$P(x) = \{1.953 \times 10^{-8}(18 + 3x)^{1/2}\}\,. \tag{17}$$

From (16) and (17) the effective mass can be calculated by $m_c = 3\hbar^2 E_g/4P^2$.

The optical dielectric function $\varepsilon_{opt}(x)$ is a crucial parameter for the polar-optical scattering probability, determining the mobility in the high temperature region.

The two different expressions,

$$\varepsilon_{opt}(x) = 15.2 - 13.7x + 6.4x^2 \qquad [16], \tag{18a}$$

$$\varepsilon_{opt}(x) = \frac{3.15x}{G - 1}; \qquad G = \frac{(2.785 + 0.768x)^2}{(2.884 - 0.178x)^2} \qquad [3], \tag{18b}$$

result in a difference of the high temperature mobility by 1.7 for $x = 0.2$. The same holds for the static dielectric function $\varepsilon_s(x)$,

$$\varepsilon_s(x) = 20.5 - 15.5x + 5.7x^2 \qquad [16], \tag{19a}$$

$$\varepsilon_s(x) = \varepsilon_{opt}(x) + 5.71(1 - x) + 3.15x \qquad [3]. \tag{19b}$$

In order to calculate the carrier densities very quickly, an interpolation formula of Stahl [17] for the modified Fermi integral $J_{1/2}$

$$J_{1/2}(\eta, \xi) = \frac{2}{\sqrt{\pi}} \int_0^\infty dx \, \frac{[x(1 + \xi x)]^{1/2} (1 + 2\xi x)}{1 + \exp(x - \eta)} \tag{20}$$

($\xi = kT/E_g$) has been used, which differs from the exact result by less than 1% in the region $\xi = [0 \text{ to } 0.1]$. The first derivative of this interpolation formula was used to determine the screening length after (5′)

The mobility of heavy holes depends on their effective mass. Values between $0.4m_0$ and $0.7m_0$ can be found in the literature.

A list of implemented functions and constants:

$\varepsilon_{opt}(x)$ [16], [3] optional
$\varepsilon_s(x)$ [16], [3] optional
m_{hh} optional (standard $0.5m_0$ [16])
r_0 optional (standard 5×10^{-8} cm)
N_t optional (standard 1×10^{18} cm^{-3})
$\varkappa$ optional (standard 0.1)
ΔE_c optional (standard 1.1 eV [18])
ΔE_v optional (standard 0.3 eV [18])
E_t $0.4 \times E_g(x, T)$
N_0 $2/d^3$, $d = 3.231 \times 10^{-8}$ cm [2]
E_1 2.7 eV [2]
$\bar{M}$ $\{21.19 + 18.666x + 33.31(1 - x)\} \times 10^{-26}$ kg [2]
ϱ $\bar{M}N_0/2$
γ_{pz}^2 9×10^7 kg/ms^2 [2]
c_l 2.8×10^3 m/s [2]
ω_{LO1} $(2.633 - 0.192x) \times 10^{13}$ s^{-1}
ω_{LO2} $(2.785 + 0.768x) \times 10^{13}$ s^{-1}
ω_{TO1} $(2.257 + 0.158x) \times 10^{13}$ s^{-1}
ω_{TO2} $(2.884 - 0.178x) \times 10^{13}$ s^{-1}
} $(0.1 \leqq x \leqq 0.4)$ [3]

4. Fit to Hall Data

To check the validity of the model the theoretical results were fitted to experimental data of the electron and hole Hall mobilities [19, 3] over the whole temperature range. The contribution of light holes has been switched off in the fitting procedure. This is due to the large ratio of the effective densities of states of heavy and light holes $N_{hh}/N_{lh} > 10^2$ and due to the fact that the influence of light holes both on the po and cc mobility is negligible, as shown by other authors [21, 22].

No difference between the drift and Hall mobility is obtained, if the Kohler variational method of first order is applied. Therefore, the Hall factors both for impurity scattering and for the high temperature po-scattering were calculated to be more consistent at least in the low and high temperature ranges. Including Fermi statistics and Kane band structure the calculation of the Hall factor gives

$$r = \frac{3}{2}\frac{n}{N_c}\exp(-\eta_c/kT)\frac{\langle x\tau^2\rangle_\xi}{\langle x\tau\rangle_\xi^2}, \qquad x = \frac{E}{kT}, \tag{21}$$

with the average

$$\langle G\rangle_\xi = \frac{2}{\sqrt{\pi}}\exp(-\eta_c/kT)\int_0^\infty \mathrm{d}x\, x^{1/2}\frac{(\xi x+1)^{3/2}}{2\xi x+1} f(x)[1-f(x)]\,G(x), \tag{22}$$

which turns into the well-known Maxwell average in the case of Boltzmann statistics and parabolic bands. Inserting the relaxation time τ into (21) one can estimate the difference between Hall and drift mobilities in the temperature ranges of interest.

The electron and hole Hall factors as a function of inverse temperature are shown in Fig. 1. Below 200 K the Hall factor both for electrons and holes is determined by the cc-scattering and is almost constant (1.75) in the case of the nondegenerated hole gas. In contrast, the electron Hall factor for $N_D = 7\times10^{15}\,\mathrm{cm}^{-3}$ is about 2.3 in the intermediate

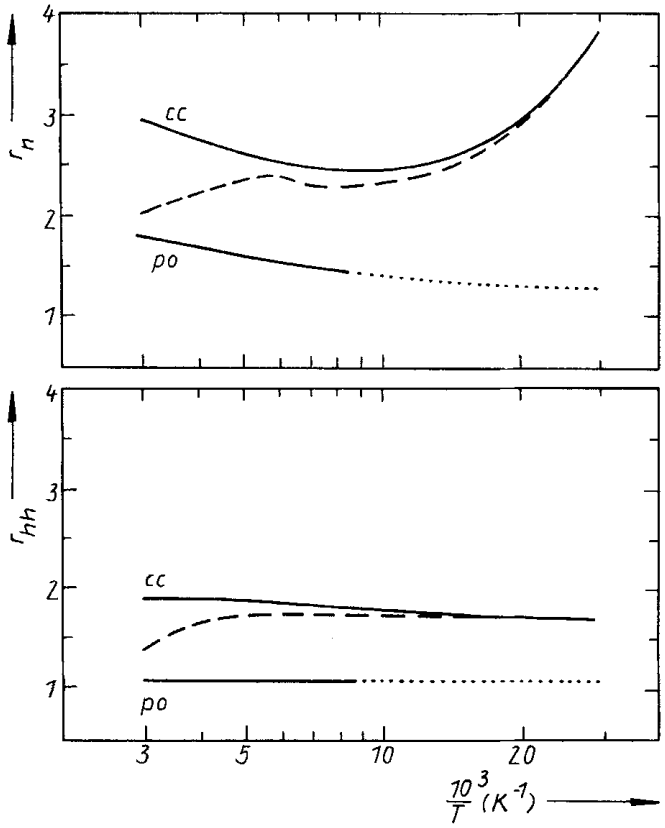

Fig. 1. Electron (upper part, $N_D = 7\times10^{15}\,\mathrm{cm}^{-3}$) and heavy hole (lower part, $N_A = 1\times10^{16}\,\mathrm{cm}^{-3}$) Hall factors vs. inverse temperature for cc-scattering and high temperature po-scattering. The resulting Hall factors are indicated with dashed lines. Parameters: $x = 0.22$, uncompensated

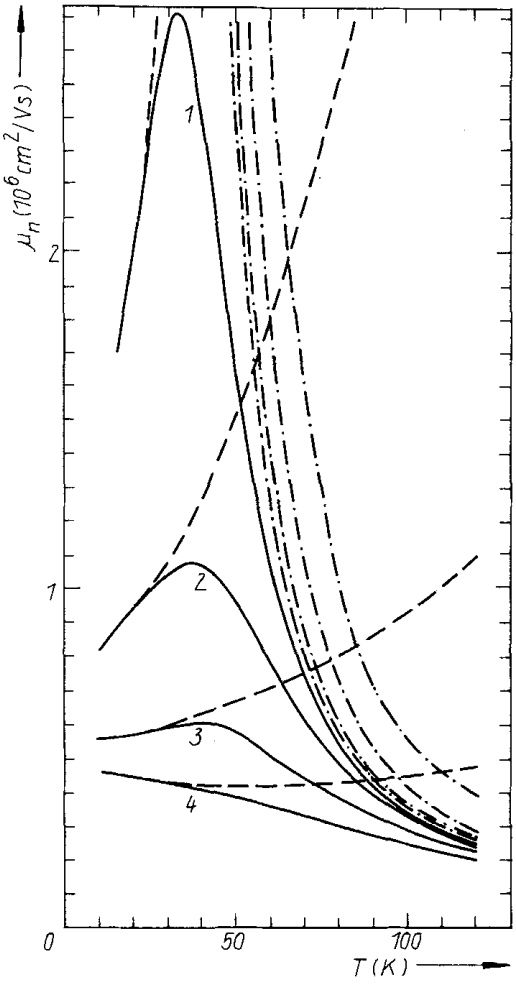

Fig. 2. Electron mobility vs. temperature including po- and cc-scattering (——— res, — — — cc, ·—·—·po). Parameters: $Hg_I = V_{Hg} = 0$, $A_{res} = 1 \times 10^{12}$ cm^{-3}, $x = 0.22$, ε after [16]. (1) $D_{res} = 8 \times 10^{13}$, (2) 4×10^{14}, (3) 2×10^{15}, (4) 1×10^{16} cm^{-3}

temperature range and tends to

$$r \to 1 + 2\frac{h_c}{E_g} \tag{23}$$

for high degeneracy, i.e. it follows linearly the Fermi level there.

The fit to experimental Hall data is based on the impurity model proposed by Höschl et al. [3] containing Hg interstitials (Hg_I) and residual donors (D_{res}) as source of electrons, but Hg vacancies (V_{Hg} at $0.7E_g$ and 6 meV) and residual acceptors (A_{res} at 12 meV) as source of holes.

In Fig. 2 the theoretical electron drift mobility over the temperature is shown for different doping concentrations assuming only residual impurities. An increasing doping concentration is followed by a transition from the nondegenerated to the degenerated range and changes the mobility curve qualitatively. Only cc- and po-scattering have been taken into account in Fig. 2. The cc mobility curve becomes flatter with rising carrier density and almost constant for high degeneracy. As a result, the low temperture electron mobility for high electron densities is expected to become constant. This is confirmed by measurements [19, 20], but can also be verified analytically specializing (13) to cc-scattering and to the case of high degeneracy by replacing the derivative of the Fermi function by a δ-function.

The theoretical hole drift mobility, with cc- and po-scattering (upper curve) and additionally nc-scattering (lower curve), is shown in Fig. 3 as a function of temperature. If the nc-scattering dominates (lower curve), the mobility is dropped down and the maximum is quenched. Meyer et al. [9] have discussed various additional scattering mechanisms to explain the measured low hole mobilities at low temperatures, which are in contradiction with measured doping concentrations when only cc-scattering is assumed.

Fig. 4a and b exhibit how the fit to experimental data [19] can be improved, if the nc- and sf-scattering are included. The nc-scattering alone flattens the curve but makes it strongly asymmetrical due to its $T^{-\alpha}$-behaviour ($\alpha \geqq 1/2$). If the sf-scattering is incorporated ($\mu^{sf} \sim T^{1/2}/m^{*3/2}$), the crossing point of the nc- and sf-mobility curves can be shifted toward lower temperatures by a proper choice of the parameters r_0, $\varkappa$, N_t, and E_t. Consequently, the drop of the total mobility curve is more symmetrical then.

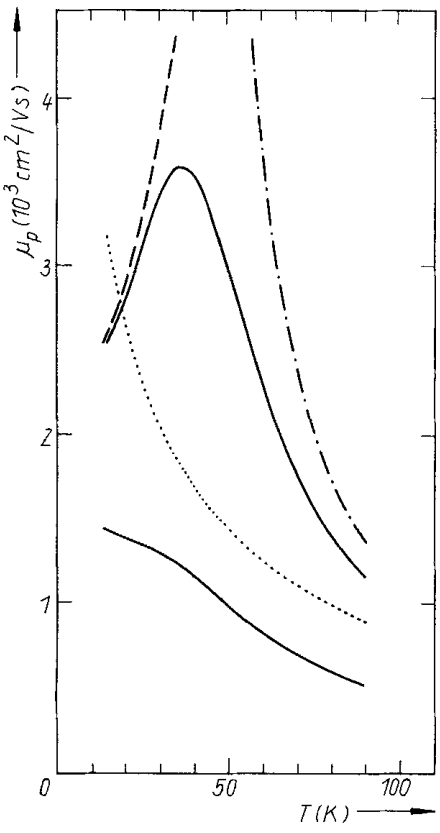

Fig. 3. Hole mobility without (upper curve) and with nc-scattering (lower curve) vs. temperature (——— res, — — — cc, ·—·—· po, ····· nc). Parameters: $A_{res} = 9 \times 10^{15}$ cm^{-3}, $D_{res} = 2 \times 10^{14}$ cm^{-3}, $N_t = 1 \times 10^{18}$ cm^{-3}, $\varkappa = 0$, $r_0 = 1.3 \times 10^{-7}$ cm, other parameters cf. Fig. 2

In Fig. 4c two measured samples of [3] with the composition and doping parameters given there and the corresponding Hall factor of about 1.75 are compared with the present model. The po-, cc-, and alloy scattering were taken into account. The disagreement is within a factor 2, but the fit could be improved by changing the heavy hole mass and/or the value of the dielectric function.

Fig. 5 shows an example of a fit to measured electron Hall mobilities [19], intentionally leaving out the Hall factor. It turns out that the high temperature branch cannot be reproduced without taking into account nc-scattering. On the other hand, the inclusion of the Hall factor would result in an increase of the low temperature mobility, which has never been observed. That could indicate a Fermi level pinning to the band edge.

In this section the action of various physical parameters of the model was demonstrated. The achieved fit should be sufficient for a further application of the mobility routine in a device simulation program. The physical significance, however, is restricted by several uncertainties, like the Kohler method itself, the matrix elements, the Hall factor, and some of the material parameters, like the heavy hole mass and the dielectric constants. Two peculiarities are supposedly outside these limitations: the sharpness of the hole mobility curve versus inverse temperature and the strong deviation of calculated high temperature electron mobilities from the measured ones. At the very least a scattering process with a temperature dependence like that of the nc-mobility is able to moderate these deviations.

5. Drift Mobility Profiles of a Model Structure

A n^+n^-p-profile of completely ionized residual impurities has been assumed to demonstrate the spatial variability of the mobility in HgCdTe. The doping profile serves as a model for real infrared detector diodes. Only cc- and po-scattering have been taken into consideration.

Fig. 6a shows that in the case of electrons the cc-scattering dominates over the whole structure at 77 K ($N_A = 9 \times 10^{15}$ cm^{-3}). The total electron mobility varies over one order of magnitude (5×10^4 to 5×10^5 cm^2/Vs).

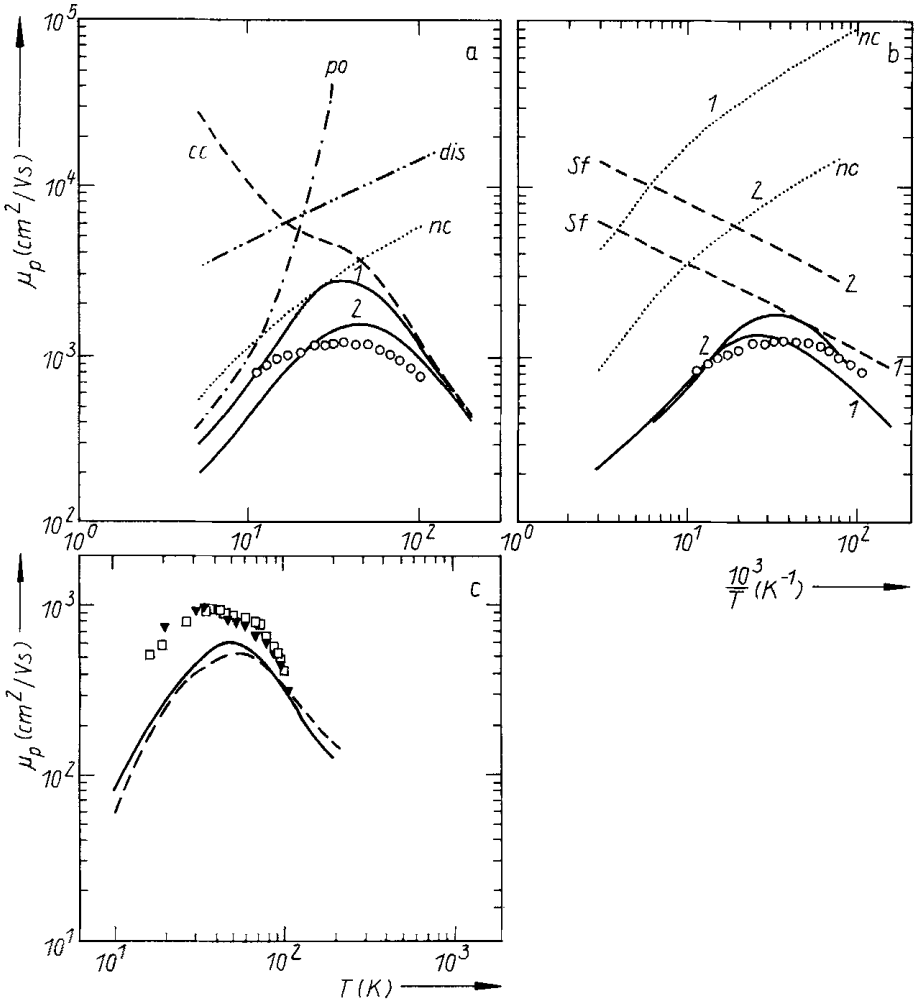

Fig. 4. Hole mobility vs. reciprocal temperature a) without (1) and with (2) nc-scattering; b) with nc- and sf-scattering. (1) $r_0 = 7.6 \times 10^{-8}$ cm, $\varkappa = 0.65$; (2) $r_0 = 1 \times 10^{-7}$ cm, $\varkappa = 0.43$. Parameters: $p(77\text{ K}) = 1 \times 10^{16}\text{ cm}^{-3}$, $Hg_I = 5 \times 10^{14}\text{ cm}^{-3}$, $V_{Hg} = 1 \times 10^{15}\text{ cm}^{-3}$, $D_{res} = 2 \times 10^{14}\text{ cm}^{-3}$, $A_{res} = 1.15 \times 10^{16}\text{ cm}^{-3}$, $m_{hh} = 0.5m_0$, ε after [16], $x = 0.22$, $r_0 = 1.2 \times 10^{-7}$ cm, $N_t = 1 \times 10^{18}\text{ cm}^{-3}$, $E_t = E_g(x, T)/2$, $\Delta E_v = 0.3$ eV. Experimental points: sample TH 362-21_{t121} with $p(77\text{ K}) = 1.18 \times 10^{16}\text{ cm}^{-3}$ [19]. c) Comparison of the present model with two samples of [3]: □, — — — $x = 0.201$, $V_{Hg} = 6.7 \times 10^{16}\text{ cm}^{-3}$, $A_{res} = 3 \times 10^{16}\text{ cm}^{-3}$, $D_{res} = 4.4 \times 10^{16}\text{ cm}^{-3}$; ▼, ——— $x = 0.222$, $V_{Hg} = 3 \times 10^{16}\text{ cm}^{-3}$, $A_{res} = 1.2 \times 10^{16}\text{ cm}^{-3}$, $D_{res} = 2.5 \times 10^{16}\text{ cm}^{-3}$; po-, cc-, and alloy scattering taken into account. Parameters: $m_{hh} = 0.7m_0$, ε after [3], $\Delta E_v = 0.3$ eV

In the case of holes (Fig. 6b) the cc-scattering is dominant only in the heavily doped n^+-region. In the n^-- and p-regions the hole mobility is determined by the po-scattering and is almost constant there. Within the whole structure the hole mobility varies over one order of magnitude (70 to 600 cm^2/Vs).

Since the operation of photodiodes depends on the minority carriers, the spatial variability of both drift mobilities should have a marked effect in device simulation. This effect will be discussed in a subsequent paper.

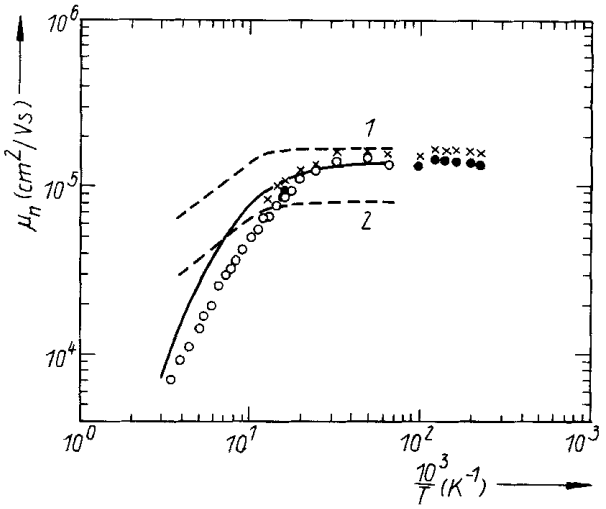

Fig. 5. Electron mobility vs. reciprocal temperature including po- and cc-scattering (1) and (2) and additionally nc-scattering (solid line). Parameters: $x = 0.232$, $N_t = 1 \times 10^{18}$ cm^{-3}, $V_{Hg} = D_{res} = 0$. (1) $Hg_I = 3.6 \times 10^{15}$ cm^{-3}, $A_{res} = 0$, n(77 K) $= 7.2 \times 10^{15}$ cm^{-3}, ε after [16]; (2) $Hg_I = 5 \times 10^{15}$ cm^{-3}, $A_{res} = 2.5 \times 10^{15}$ cm^{-3}, n(77 K) $= 7.5 \times 10^{15}$ cm^{-3}, ε after [3]; ——— $Hg_I = 3.65 \times 10^{15}$, ε after [16], other parameters cf. (1), $r_0 = 2 \times 10^{-7}$ cm, $E_t = E_g(x, T)/2$, n(77 K) $= 7.3 \times 10^{15}$ cm^{-3}; experimental points: sample 298_{t326}(LPE on n-material) with n(77 K) $= 7.3 \times 10^{15}$ cm^{-3} for different magnetic field strengths (● $B = 0.006$, × 0.034, ○ 0.01 T) [19]

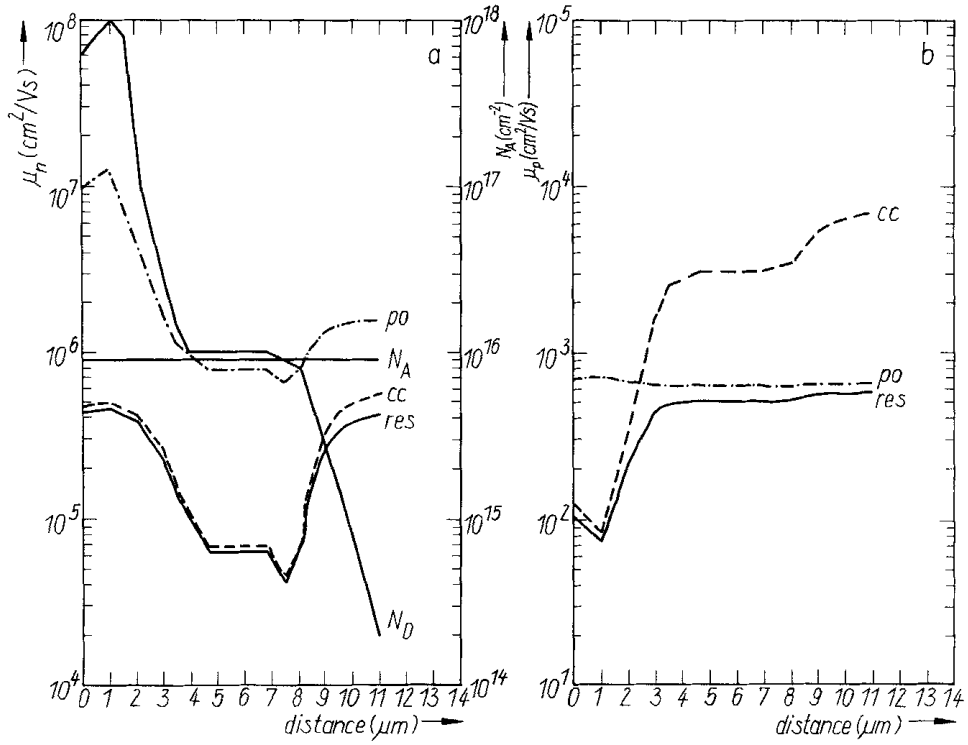

Fig. 6. a) Electron mobility profile of a n^+n^-p-junction model with indicated doping profile ($N_A = A_{res}$, $N_D = D_{res}$). Only po- and cc-scattering have been included. Parameters: $x = 0.2$, $T = 77$ K, ε after [3]. b) Hole mobility profile of the n^+n^-p-junction model of Fig. 6a. $m_{hh} = 0.7m_0$, other parameters cf. Fig. 6a

6. Conclusions

In this paper a microscopic model of the drift mobility $\mu(T, x, N_{dop}(\boldsymbol{r}), n(\boldsymbol{r}), p(\boldsymbol{r}))$ in $Hg_{1-x}Cd_xTe$ ($x \approx 0.2$) was established on the basis of the Kohler variational method. It represents a medium level of quantum-mechanical description remaining applicable in 2D numerical device simulation. All input parameters have a definite physical meaning. The special situation in the mixed crystal HgCdTe with alloy scattering and implantation related structural defect profiles is reflected and degeneracy effects are completely included. A sufficient agreement with experimental Hall data could be achieved. Changing the microscopic parameters the model can also be applied to other materials. In a n^+n^-p-photodiode both drift mobilities have been shown to vary over one order of magnitude.

References

[1] W. Brauer and H.-W. Streitwolf, Theoretische Grundlagen der Halbleiterphysik, Akademie-Verlag, Berlin 1977 (p. 166).
[2] J. J. Dubowski, T. Dietl, W. Szymanska, and R. R. Gałazka, J. Phys. Chem. Solids **42**, 351 (1981), and references therein.
[3] P. Höschl, P. Moravec, V. Prosser, V. Szöcs, and R. Grill, phys. stat. sol. (b) **145**, 637 (1988).
[4] G. Lucovski, Solid State Commun. **3**, 299 (1965).
[5] P. A. Fedders, J. appl. Phys. **54**, 1804 (1983).
[6] V. L. Bonč-Bruevič, and S. G. Kalashnikov, Halbleiterphysik, Deutscher Verlag der Wissenschaften, Berlin 1982 (p. 433).
[7] J. W. Harrison and J. R. Hauser, J. appl. Phys. **47**, 293 (1976).
[8] J. W. Harrison and J. R. Hauser, Phys. Rev. B **13**, 5347 (1976).
[9] J. R. Meyer, F. J. Bartoli, and C. A. Hoffman, J. Vacuum Sci. Technol. A **5**, 3035 (1987).
[10] L. Makowski and M. Glicksman, J. Phys. Chem. Solids **34**, 487 (1973).
[11] J. Kossut, phys. stat. sol. (b) **86**, 539 (1978).
[12] W. Szymanska and T. Dietl, J. Phys. Chem. Solids **39**, 1025 (1978).
[13] J. R. Meyer and F. J. Bartoli, Phys. Rev. B **23**, 5413 (1981).
[14] J. Chu, S. Xu, and D. Tang, Appl. Phys. Letters **43**, 1064 (1983).
[15] J. D. Wiley and R. N. Dexter, Phys. Rev. **181**, 1811 (1969).
[16] R. Dornhaus and G. Nimtz, Solid State Phys. **78**, 1 (1976).
[17] M. Stahl, unpublished.
[18] K. C. Hass, H. Ehrenreich, and B. Velicky, Phys. Rev. B **27**, 1088 (1983).
[19] W. Hoerstel and A. Schmiede, private communication.
[20] E. Finkman and Y. Nemirovski, J. appl. Phys. **53**, 1052 (1982).
[21] D. Kranzer, J. Phys. C **6**, 2967 (1973).
[22] G. L. Bir, E. Normantas, and G. Pikus, Fiz. tverd. Tela **4**, 1180 (1962); Soviet Phys. – Solid State **4**, 867 (1962).

(Received March 28, 1990; in revised form July 20, 1990)